Available online at www.sciencedirect.com
ScienceDirect
Journal of Theoretical Biology 244 (2007) 388–399
Journal of Theoretical Biology
www.elsevier.com/locate/yjtbi

Cell resensitization after delivery of a cycle-specific anticancer drug and effect of dose splitting: Learning from tumour cords

A. Bertuzzi[a,*], A. Fasano[b], A. Gandolfi[a], C. Sinisgalli[a]

[a]*Istituto di Analisi dei Sistemi ed Informatica del CNR, Viale Manzoni 30, 00185 Roma, Italy*
[b]*Dipartimento di Matematica "U. Dini" Università degli Studi di Firenze, Viale Morgagni 67/A, 50134 Firenze, Italy*

Available online 16 September 2006

Abstract

After a single dose of an anticancer agent, changes due to cell death are expected to occur in the distribution of cells between proliferating and quiescent compartment as well as in the oxygenation and nutritional state of surviving cells. These changes are transient because tumour regrowth tends to restore the pretreatment status. The reoxygenation due to the decrease of oxygen consumption is expected to induce cell recruitment from quiescence into proliferation, and consequently to increase the sensitivity of the cell population to a successive treatment by a cycle-specific drug. In previous papers we proposed a model of the response of tumour cords (cylindrical arrangements of tumour cells growing around a blood vessel of the tumour) to single-dose treatments. The model included the motion of cells and oxygen diffusion and consumption. On the basis of that model suitably extended to better account for the action of anticancer drugs, we study the time course of the oxygenation and of the redistribution of cells between the proliferating and quiescent compartments. By means of simulations of the response to a dose delivered as two spaced equal fractions, we investigate the dependence of tumour response on the spacing between the fractions and on the main parameters of the system. A time window may be found in which the delivery of two fractions is more effective than the delivery of the undivided dose.

Keywords: Chemotherapy; Drug scheduling; Reoxygenation; Cell recruitment; Tumour cords

1. Introduction

Delivery of a single dose of an anticancer drug is expected to cause a redistribution of tumour cells between the proliferating and the quiescent compartment and among the cell-cycle phases, since most drugs are mainly effective on cycling cells possibly with some phase specificity. Moreover, cell death is expected to produce a decrease in the consumption of oxygen and nutrients and then induce changes in the oxygenation and nutritional state of the surviving cells. These changes will be transient because tumour regrowth tends to restore the pretreatment status. Hahnfeldt et al. (2003) proposed a mathematical ODE model for chemotherapy in which the tumour cell population was composed by two subpopulations having different sensitivities to the drug, with constant transition rates regulating the balance between these subpopulations. In the case of a single bolus treatment, the model predicted that the overall sensitivity of the cell population would recover the pretreatment level (*cell resensitization*) after a transient refractory phase due to the survival of the less sensitive cells. The authors used the model to discuss the advantages of a low-dose dose-dense protocol. Previously, the implications of the heterogeneity of cell sensitivity had been investigated in the context of radiotherapy (Brenner et al., 1995; Hahnfeldt and Hlatky, 1998).

We observe, however, that the reoxygenation of hypoxic regions occurring after treatment (Olive, 1994; Masunaga et al., 2000) is likely to force cell recruitment from quiescence into proliferation. Evidences of cell recruitment have been found after a single dose of radiation (Potmesil and Goldfeder, 1980; Nakano and Oka, 1991; Masunaga et al., 1993). Consequently, the cell population might exhibit an *increased* sensitivity to a successive treatment by cycle-specific drugs, as compared to the pretreatment

*Corresponding author.
E-mail addresses: bertuzzi@iasi.cnr.it (A. Bertuzzi), fasano@math.unifi.it (A. Fasano), gandolfi@iasi.cnr.it (A. Gandolfi), sinisgalli@iasi.cnr.it (C. Sinisgalli).

0022-5193/$ - see front matter © 2006 Elsevier Ltd. All rights reserved.
doi:10.1016/j.jtbi.2006.08.025

sensitivity. In the present paper, we intend to investigate the resensitization process by taking into account the dynamics of oxygenation in an ideal model of tumour vasculature, that is, in an array of tumour cords.

In previous papers (Bertuzzi et al., 2003, 2004) we proposed a model of the response of tumour cords (cylindrical arrangements of tumour cells growing around blood vessels of the tumour) to single-dose treatments. The model included the spatial distribution of cells, cell motion, and oxygen diffusion and consumption. On the basis of that model, suitably extended to more adequately account for the action of anticancer drugs, we study here the time course of the oxygenation and of the redistribution of cells between the proliferating and the quiescent compartment. In Sections 2–4 we discuss the general modelling assumptions, the tumour cord model, and its steady state. Section 5 presents the simulations of the model response to a single dose of drug and the time course of cell resensitization. By means of simulations of the response to a total dose delivered as two spaced equal fractions, we investigate in Sections 6 and 7 the dependence of tumour response on the spacing between these fractions. A time window may be found in which the delivery of two fractions is more effective than the delivery of the single undivided dose.

2. General assumptions

2.1. Regulation of cell kinetics by oxygen and nutrients

In tumour cell populations, the oxygen tension and the concentration of nutrients such as glucose, are known to affect the progression across the cell cycle, their decrease possibly causing cell-cycle arrest and the consequent establishing of the quiescence status. At very low concentrations of these chemicals cell death occurs. In vivo estimates of the percentage of S-phase cells in different zones of tumour cords, obtained by pulse injection of ^{3}H-thymidine, have shown that cell proliferation slows down when moving toward cord periphery, and this fact has been related to the decay of nutrient concentration (Tannock, 1968; Hirst and Denekamp, 1979; Moore et al., 1984). Similar findings have been reported for in vitro multicellular spheroids, in which the S-phase fraction was found to decrease at increasing depth into the viable rim (Freyer and Sutherland, 1986b; Bredel-Geissler et al., 1992). Freyer and Sutherland (1986a, b) and Casciari et al. (1992) evidenced that both oxygen and glucose concentrations in the medium affect the decrease of cell proliferation and the thickness of the viable rim, suggesting the mutual role of their deprivation in inducing cell death. By detecting the proliferation marker Ki67 and the label iododeoxyuridine, Neshasteh-Riz et al. (1997) have shown that the fraction of nonproliferating cells, which is nonzero also in the proximity of the spheroid surface, grows gradually inwards. Reoxygenation and serum refeeding of in vitro cell lines have been found to induce recruitment of quiescent cells into proliferation (Åmellem and Pettersen, 1993; Bakker et al., 1993). Recently, the molecular mechanisms of the cell response to oxygen deprivation came to be elucidated, and Alarcón et al. (2004) incorporated the effect of hypoxia in a mathematical model of cell-cycle control.

Although oxygen, glucose and other chemicals appear to interact in a complex way in determining the proliferative status of cells and the occurrence of cell death, we will consider only one species of nutrient that regulates cell kinetics and is also critical for cell viability. In the following, we will identify this chemical with oxygen and denote its concentration by σ, with no distinction between intracellular and extracellular concentration. We divide the viable cell population into proliferating (P) and quiescent (Q) cells and, as in Friedman (2004) and in Bertuzzi et al. (2005b), we assume that cells can undergo transitions from one state to the other with transitions rates dependent on σ. A simplified representation of the proliferating cell population is adopted, disregarding the cell age or the structure of the cell cycle. Let us denote by $\lambda(\sigma)$ and $\gamma(\sigma)$, respectively, the transition rate from proliferation into quiescence and the transition rate from quiescence into proliferation: λ and γ will be a nonincreasing and, respectively, a nondecreasing function of σ. In particular, we assign two threshold values for σ, $\sigma_P > \sigma_Q$, and we assume: $\lambda = \lambda_{max}$ and $\gamma = \gamma_{min}$ for $\sigma \leqslant \sigma_Q$, $\lambda = \lambda_{min}$ and $\gamma = \gamma_{max}$ for $\sigma \geqslant \sigma_P$, with $\lambda_{max} > \lambda_{min} \geqslant 0$ and $\gamma_{max} > \gamma_{min} \geqslant 0$. $\lambda(\sigma)$ decreases linearly and $\gamma(\sigma)$ increases linearly in the interval (σ_Q, σ_P) (see Fig. 1A). Although the experimental data suggest a decrease of the rate of progression across the cell cycle as the nutrient concentration decreases, for simplicity we take a constant proliferation rate χ independent of σ. A more complex mechanism for the recruitment of quiescent cells into proliferation was considered in Bertuzzi et al.

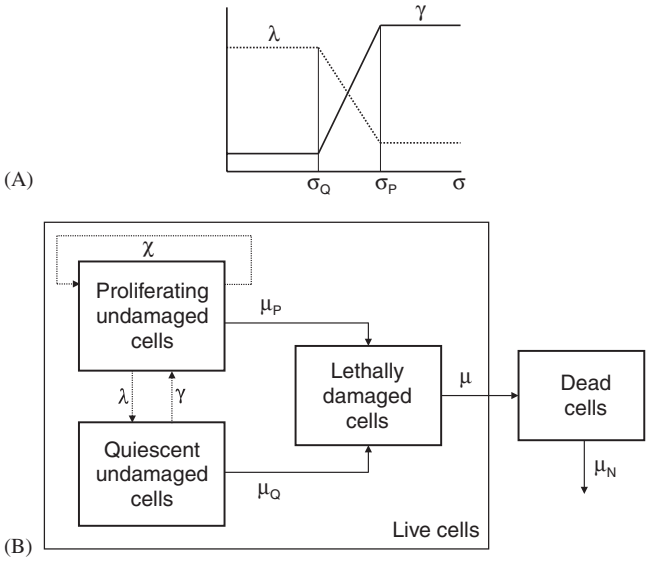

Fig. 1. (A) Profile of the functions $\lambda(\sigma)$ and $\gamma(\sigma)$ that govern the transitions from proliferation into quiescence and, respectively, from quiescence into proliferation. (B) Block diagram illustrating the activity of the cytotoxic drug. Symbols explained in the text.

(2005a) where, supposing that cells become quiescent if oxygen concentration falls below a given threshold, the recovery of proliferation when oxygen concentration increases occurs with a delay depending on the time spent by the cell into quiescence.

To illustrate the kinetic behaviour of a cell population under the above assumptions (neglecting for the moment the spatial structure that, as we will see, limits the growth), let us consider a cell population able to grow unboundedly in a homogeneous environment characterized by an assigned σ value (then λ and γ will be constant). Let $N_P(t)$ and $N_Q(t)$ denote the number of proliferating and, respectively, quiescent cells at time t. According to the above assumptions, we have

$$\dot{N}_P = \chi N_P - \lambda N_P + \gamma N_Q, \tag{1}$$

$$\dot{N}_Q = \lambda N_P - \gamma N_Q. \tag{2}$$

If $\gamma > 0$, the linear system (1)–(2) has one positive and one negative eigenvalue given by

$$\alpha_\pm = \tfrac{1}{2}[(\chi - \lambda - \gamma) \pm \sqrt{(\chi - \lambda - \gamma)^2 + 4\chi\gamma}], \tag{3}$$

and it can be seen that the eigenvector corresponding to α_+ has positive components. Thus the population will have asymptotically an asynchronous exponential growth, and both N_P, N_Q will go to $+\infty$ irrespective of the sign of $\chi - \lambda$. If $\gamma = 0$ (no recruitment) the growth is assured by the condition $\chi \geqslant \lambda$.

Denoting by y the proliferating fraction, that is, the ratio between the number of proliferating cells and the total number of cells, from Eqs. (1)–(2) we obtain

$$\dot{y} = \chi y(1 - y) - \lambda y + \gamma(1 - y), \tag{4}$$

and asymptotically the proliferating fraction will attain the value

$$y_\infty = \frac{1}{2}\left[\left(1 - \frac{\lambda + \gamma}{\chi}\right) + \sqrt{\left(1 - \frac{\lambda + \gamma}{\chi}\right)^2 + 4\frac{\gamma}{\chi}}\right]. \tag{5}$$

Thus, if $\sigma > \sigma_P$ and $\lambda = \lambda_{min} = 0$, it is $y_\infty = 1$. By contrast, if $\sigma < \sigma_Q$ and $\gamma = \gamma_{min} = 0$, we have $y_\infty = 1 - \lambda_{max}/\chi$ if $\lambda_{max} < \chi$ and $y_\infty = 0$ if $\lambda_{max} \geqslant \chi$. Eq. (4) provides some insight into the population behaviour following a stepwise change in the nutrient concentration and then in the λ and γ values. Let us assume that the proliferating fraction has initially the value given by (5). If σ decreases from a value larger than σ_P to a value smaller than σ_Q and $\lambda_{min} = 0$, y will decrease from the unity toward the new asymptotic value with initial slope λ_{max}. Conversely, if σ increases from a value smaller than σ_Q to a value larger than σ_P and $\gamma_{min} = 0$, the proliferating fraction will increase toward the new asymptotic value with initial slope γ_{max} if $\lambda_{max} \geqslant \chi$ or $\gamma_{max} + (1 - \lambda_{max}/\chi)(\lambda_{max} - \lambda_{min} - \gamma_{max})$ if $\lambda_{max} < \chi$.

2.2. Modelling the activity of cytotoxic drugs

Anticancer drugs induce cytostatic effects (i.e. blocks of the cell-cycle progression in different cell-cycle phases) and cytotoxic effects (i.e. cell death) on tumour cells. In vitro experiments in which tumour cells were exposed to drugs for a short time period, have shown that both these effects extend beyond the incubation time (Montalenti et al., 1998; Sena et al., 1999). We will consider only cycle-specific drugs, that is, drugs that affect mainly or exclusively the proliferating cells.

To account for the occurrence of cell death at later times after drug removal, we assume that the exposure to the drug induces a lethal damage in a fraction of cells, that undergo cell-cycle arrest and will die at a subsequent time. Thus the living tumour cells at a given time will be subdivided into undamaged cells and live but lethally damaged cells (see Fig. 1B). The transition into the compartment of lethally damaged cells occurs according to a rate which is a function of drug concentration. Lethally damaged cells are assumed to die following a first-order kinetics.

A similar mechanism for the description of the kinetics of cell death after drug exposure was proposed by Kozusko et al. (2001) to analyse data of in vitro treatment of tumour cells. Lankelma et al. (2003) related the actual death rate to a quantity, the amount of damage, whose dynamics is controlled by a damage induction rate dependent on the drug concentration and contrasted by a first-order repair. The cell response to drug, as proposed in the present paper, can also be related to the model for the drug-induced cell death rate proposed in Bertuzzi et al. (2003).

3. Tumour cord model

Let us consider an array of tumour cords inside the tumour mass, each cord being separated from the others by a region of necrosis (see Fig. 2). We describe the generic cord as a circular cylinder around a straight central blood vessel. We denote by r the radial distance from the axis, by r_0 the radius of the central vessel, and by $\rho_N(t)$ the cord

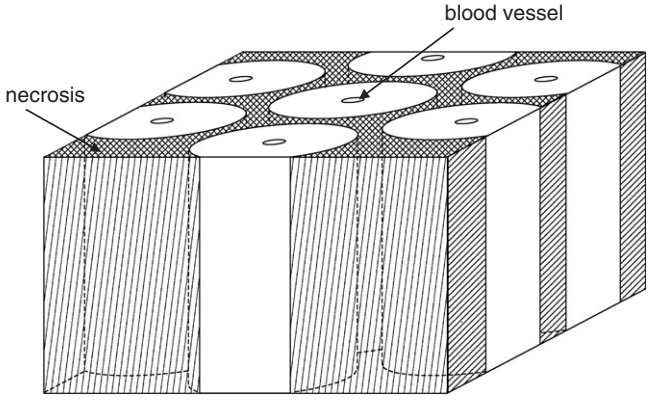

Fig. 2. Schematics of a (regular) array of tumour cords. Each vessel is surrounded by a cord of living cells immersed in a necrotic region.

radius, i.e. the interface with the necrotic region. In the cord we will distinguish: undamaged proliferating and quiescent cells, lethally damaged cells, dead cells, and extracellular fluid. Under the continuum hypothesis, we consider the volume fractions occupied locally by these components, denoting these fractions as v_P, v_Q, $v^\dagger$, v_N and, respectively, v_E (with $v_P+v_Q+v^\dagger+v_N+v_E=1$). We assume that the treatment does not affect the tumour vasculature in the time horizon considered.

The main assumptions of the cord model are summarized as follows: (i) Rotational symmetry is assumed, and all the model variables are independent of the axial coordinate. (ii) Cell velocity is radially directed. Neglecting the longitudinal cell motion is a simplification which is justifiable away from the ends of the cord. The dominance of the radial cell migration in tumour cords has already been suggested by Tannock (1968). (iii) The transition rates between the proliferating and the quiescent state are regulated by the oxygen concentration as described in Section 2.1. (iv) We assume that cells die instantaneously when σ falls to a critical value $\sigma_N<\sigma_Q$. The occurrence of a delay between the instant at which $\sigma=\sigma_N$ for a cell and the actual cell death has been explored by Bertuzzi et al. (2005a), leading to a rather complex description of the transient that has been avoided here. The spontaneous cell loss within the cord, considered in Bertuzzi et al. (2004), is here neglected (only a small percentage of dead cells has been found by Moore et al., 1984). (v) Random, dose-dependent cell death is induced by treatment, and lethally damaged cells die with a rate constant μ. (vi) Dead cells within the cord are degraded to a fluid waste at a rate μ_N. This waste will be drained away by the flow of extracellular fluid along the axial direction of the cord.

The dynamics of the mixture of cells and extracellular fluid should be described by writing the momentum balance and including the interactions among the components (see, for instance, Byrne and Preziosi, 2003). To take full advantage of the simplified geometry, we make instead the further simplifying assumptions: (vii) The velocity of the cellular component is the same for both live and dead cells. This common velocity is given by the scalar field $u(r,t)$. (viii) The volume fraction v_E of extracellular fluid is constant in space and time. In other words, it is assumed that both live and dead cells possess a uniform spatial arrangement, which is quickly recovered after any perturbation caused by cell proliferation and degradation of dead cells. These assumptions lead to a purely kinematic approach. The fluid is supplied by the central blood vessel and leaves the system through the terminal sections, driven by a pressure gradient created by the presence of distant lymphatic vessels. Although experimental measurements support assumption (viii) for tumour cords at the steady state, since the data showed small changes in cell density with the radial distance (Moore et al., 1984, 1985), this assumption becomes an oversimplification in the transient following a treatment, where there are evidences of an increased volume fraction of extracellular fluid (Zhao et al., 1996).

Assuming that all the components have equal mass density, the conservation equations for the volume fractions of live and dead cells in $r\in(r_0,\rho_N(t))$ can be written as follows:

$$\frac{\partial v_P}{\partial t}+\frac{1}{r}\frac{\partial}{\partial r}(ruv_P)=\chi v_P+\gamma(\sigma)v_Q-\lambda(\sigma)v_P-\mu_P(r,t)v_P, \quad (6)$$

$$\frac{\partial v_Q}{\partial t}+\frac{1}{r}\frac{\partial}{\partial r}(ruv_Q)=-\gamma(\sigma)v_Q+\lambda(\sigma)v_P-\mu_Q(r,t)v_Q, \quad (7)$$

$$\frac{\partial v^\dagger}{\partial t}+\frac{1}{r}\frac{\partial}{\partial r}(ruv^\dagger)=\mu_P(r,t)v_P+\mu_Q(r,t)v_Q-\mu v^\dagger, \quad (8)$$

$$\frac{\partial v_N}{\partial t}+\frac{1}{r}\frac{\partial}{\partial r}(ruv_N)=\mu v^\dagger-\mu_N v_N, \quad (9)$$

where μ_P, μ_Q are the rate constants of the lethal damaging induced by treatment on the proliferating cells and, respectively, the quiescent cells. Since from assumption (viii) $v_P+v_Q+v^\dagger+v_N=v^\star=const$, the velocity field $u(r,t)$ satisfies the equation

$$v^\star\frac{1}{r}\frac{\partial}{\partial r}(ru)=\chi v_P-\mu_N v_N, \quad u(r_0,t)=0. \quad (10)$$

Concerning the equation for σ, diffusion is the dominant transport mechanism for oxygen (and glucose) and it occurs in a quasi-stationary regime. Thus we have

$$\Delta\sigma=f(\sigma)(v_P+v_Q+v^\dagger), \quad (11)$$

with the boundary condition

$$\sigma(r_0,t)=\sigma_b, \quad (12)$$

where $f(\sigma)$ is the ratio between the consumption rate per unit volume of live cells and the diffusion coefficient, and we require $f(\sigma_N)>0$. At the inner boundary $r=r_0$, i.e. at the vessel wall, we have for simplicity prescribed the (constant) oxygen blood concentration $\sigma_b>\sigma_P$.

The interface $r=\rho_N(t)$ can be determined by noting that the necrotic material cannot be converted back to living cells and that assumption (iv) forbids to have living cells for $\sigma<\sigma_N$. Thus the following inequalities must be satisfied

$$u(\rho_N(t),t)-\dot\rho_N(t)\geqslant 0, \quad (13)$$

$$\sigma(\rho_N(t),t)\geqslant\sigma_N, \quad (14)$$

together with the no-flux condition

$$\left.\frac{\partial\sigma}{\partial r}\right|_{r=\rho_N(t)}=0. \quad (15)$$

Therefore, if the cells cross the interface $\rho_N(t)$, that is if $u(\rho_N,t)-\dot\rho_N>0$, the boundary condition accompanying (15) is

$$\sigma(\rho_N(t),t)=\sigma_N, \quad (16)$$

and the interface is a *nonmaterial* free boundary. Otherwise, the cord boundary becomes a *material* free boundary carrying the conditions (15) and

$$\dot\rho_N=u(\rho_N(t),t). \quad (17)$$

The first case occurs, for instance, in the stationary state in the absence of treatment. The switch to the material interface may happen when a sudden massive destruction of cells rapidly lowers oxygen consumption, and the interface $\rho_N(t)$ defined by (16) tends to acquire a velocity larger than $u(\rho_N(t),t)$. The new boundary is however subjected to the constraint (14) so that, if during the cord repopulation $\sigma(\rho_N(t),t)$ tends to drop below σ_N, the free boundary must become nonmaterial again. This phenomenon has been described for the first time in Bertuzzi et al. (2004) where it is discussed in detail.

By considering the nondimensional time $t'=t\chi$, it is easy to see that the dynamics of the cell subpopulations depend on the nondimensional rates λ/χ, γ/χ, μ/χ, μ_N/χ and on the nondimensional cell damaging rates $\mu'_P(r,t')=\mu_P(r,t'/\chi)/\chi$, $\mu'_Q(r,t')=\mu_Q(r,t'/\chi)/\chi$. However, in the simulations that follow we use the dimensional variables and parameters, to better convey the biological meaning of the results.

The equations for v_P, v_Q, $v^\dagger$, v_N require an initial condition but not a boundary condition at $r=r_0$, because $u(r,t)$ vanishes at r_0. We will assume as initial condition the equilibrium solution corresponding to the absence of treatment. We describe in the next section this steady state of the system.

4. The steady state in the absence of treatment

In the absence of treatment, only viable proliferating and quiescent cells are present in the cord, thus $v_P+v_Q=v^\star$ and Eq. (11) simplifies accordingly. From (6)–(7) and (10) we obtain for v_P the equation

$$u\frac{\partial v_P}{\partial r}=\chi v_P\left(1-\frac{v_P}{v^\star}\right)-\lambda(\sigma)v_P+\gamma(\sigma)(v^\star-v_P),\qquad r_0<r<\rho_N, \tag{18}$$

where $u(r)$ is given by

$$ru(r)=\frac{\chi}{v^\star}\int_{r_0}^{r} r'v_P(r')\,\mathrm{d}r'. \tag{19}$$

Note that $v_P/v^\star$ represents the *local* proliferating fraction of the cell population and, observing that the l.h.s. of (18) is the time derivative of v_P along the trajectories, it is immediate that $v_P/v^\star$ along the trajectories satisfies the same equation (Eq. (4)) satisfied by y. As expected, the solution of (18)–(19) only depends on the ratios $\lambda(\sigma)/\chi$ and $\gamma(\sigma)/\chi$.

We may consider the problem of the existence of a constant cord radius ρ_N and a time-independent solution $v_P(r)$, $u(r)$, $\sigma(r)$ that satisfies (18)–(19) together with (11) and (12), (15), (16). This means that the cell population will have constant size with a constant distribution between proliferating and quiescent cells. Existence and uniqueness of this stationary solution have been proved in Bertuzzi et al. (2005b). Eq. (18) is degenerate at $r=r_0$ because $u(r_0)=0$. However, according to our assumptions on the shape of $\lambda(\sigma)$ and $\gamma(\sigma)$, there will exist an inner region of the cord (where $\sigma>\sigma_P$) in which these transition rates are constant. Thus, it is easy to see that the solution v_P is constant and equal to

$$\hat{v}_P=\frac{v^\star}{2}\left[\left(1-\frac{\lambda_{min}+\gamma_{max}}{\chi}\right)+\sqrt{\left(1-\frac{\lambda_{min}+\gamma_{max}}{\chi}\right)^2+4\frac{\gamma_{max}}{\chi}}\right] \tag{20}$$

for $r_0<r\leqslant\rho_P$, with the radius ρ_P such that $\sigma(\rho_P)=\sigma_P$. Moreover, it can be proved that the volume fraction v_P is decreasing and remains positive in the interval $(\rho_P,\rho_N]$ even if $\gamma_{min}=0$. As a consequence, a purely quiescent region cannot exist. In Appendix A, a positive lower bound for $v_P(\rho_N)$ is derived.

The numerical solution of the steady-state problem was computed according to a procedure which suitably modifies that described in Bertuzzi et al. (2003). In all the simulations here presented the function $f(\sigma)$ has the form (Casciari et al., 1992)

$$f(\sigma)=F\frac{\sigma}{K+\sigma}. \tag{21}$$

Fig. 3A shows an example of the profile of $v_P(r)/v^\star$ for two different values of λ_{max}/χ assuming $\lambda_{min}=\gamma_{min}=0$. Since $\lambda_{min}=0$, $v_P(r)=1$ from r_0 to ρ_P, then v_P decreases, having a larger decrease for the larger value of λ_{max}/χ (see the Appendix). It can be seen that, although v_P is always positive, a region which is virtually fully quiescent can be obtained for suitable values of the parameters. In both cases, the profile of the oxygen concentration σ (and then ρ_N) is the same since we have assumed equal consumption of the proliferating and quiescent cells (see Fig. 3B). The value chosen for r_0 ($r_0=20\,\mu\mathrm{m}$) as well as the predicted ρ_N ($\rho_N=124.8\,\mu\mathrm{m}$) are in the range of the typical values for tumour cords observed in experimental tumours (Tannock, 1968; Hirst and Denekamp, 1979; Moore et al., 1984).

5. Cell resensitization after the delivery of a single dose of drug

To describe the evolution of the cord cell population after the delivery of a chemotherapeutic drug, the damaging rates μ_P and μ_Q should be expressed as a function of the drug concentration. This would require the description of drug transport from the central vessel to the cells, and of the drug binding both to the intracellular target and to nonspecific sites. Moreover, it would require the modelling of the necrotic region and its evolution, since the drug also diffuses through this region. Because of the complexity of these processes, the rates μ_P and μ_Q are simply taken here as *assigned* functions of time only, disregarding the effects of the gradients of drug concentration along the radial direction. On the other hand, we believe that this approximation does not obscure the main features of the cord response to drug as studied in the present paper. Simulations (not shown) of the cord response were made

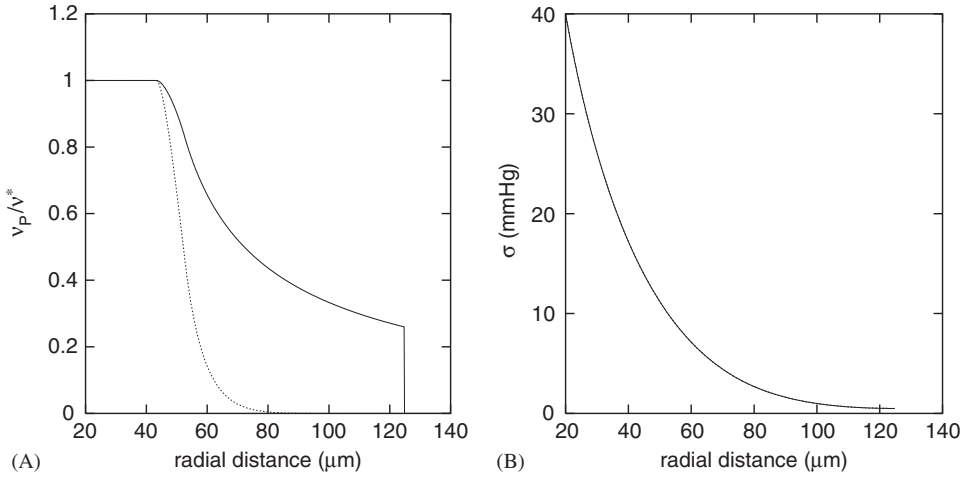

Fig. 3. (A) Normalized volume fraction of undamaged proliferating cells as a function of radial distance in the steady state; $\lambda_{max}/\chi = 1$ solid line, 4 dotted line. Parameter values (O_2 concentration in mmHg, length in μm, time in h): $\lambda_{min} = \gamma_{min} = 0$, $\gamma_{max}/\chi = 4$, $\chi = (\log 2)/24$, $\sigma_b = 40$, $\sigma_P = 15$, $\sigma_Q = 10$, $\sigma_N = 0.5$, $r_0 = 20$. Moreover $F = 0.015$, $K = 4.32$ (Casciari et al., 1992). (B) Oxygen tension as a function of radial distance.

by assuming damaging rates proportional to the nonuniform drug concentration inside the cord, as computed by a pure diffusion model without drug consumption with the necrotic region described according to Bertuzzi et al. (2003, 2004). The simulations confirmed that the cord response obtained in this way has minor differences from the one obtained when using damaging rates proportional to the drug concentration inside the vessel, at least when the effective diffusivity of the drug was larger than $10^{-7}\,\mathrm{cm}^2/\mathrm{s}$ and the time constant of the (monoexponential) drug decay was larger than 1 h.

The single-dose treatment was assumed to consist in the delivery of a single intravenous bolus of drug, and was modelled by assigning to μ_P and μ_Q the following expressions:

$$\mu_P(r,t) = \frac{m_P}{\tau_1 - \tau_2}(\mathrm{e}^{-t/\tau_1} - \mathrm{e}^{-t/\tau_2}), \tag{22}$$

$$\mu_Q(r,t) = \frac{m_Q}{\tau_1 - \tau_2}(\mathrm{e}^{-t/\tau_1} - \mathrm{e}^{-t/\tau_2}), \tag{23}$$

where m_P, m_Q represent the drug dose times the cell sensitivity to the drug. Drug decay related to elimination from the body is represented by the time constant τ_1, whereas τ_2 (that will be assumed much smaller than τ_1) represents the drug distribution time. As reference values, we have taken $\tau_1 = 3\,\mathrm{h}$ and $\tau_2 = 0.15\,\mathrm{h}$. Note that the cord response as a function of the nondimensional time $t\chi$ would depend on the nondimensional parameters $\tau_1\chi$ and $\tau_2\chi$.

Fig. 4 illustrates a typical response of the tumour cord model to a single dose of a cycle-specific drug ($m_Q = 0.2m_P$). Panel A shows the ratios between the volumes (per unit cord length) of the different subpopulations of living cells and the value of $P + Q$ at $t = 0$, for instance the ratio $\int_{r_0}^{\rho_N(t)} r v_P(r,t)\,\mathrm{d}r / \int_{r_0}^{\rho_N} r(v_P(r,0) +$

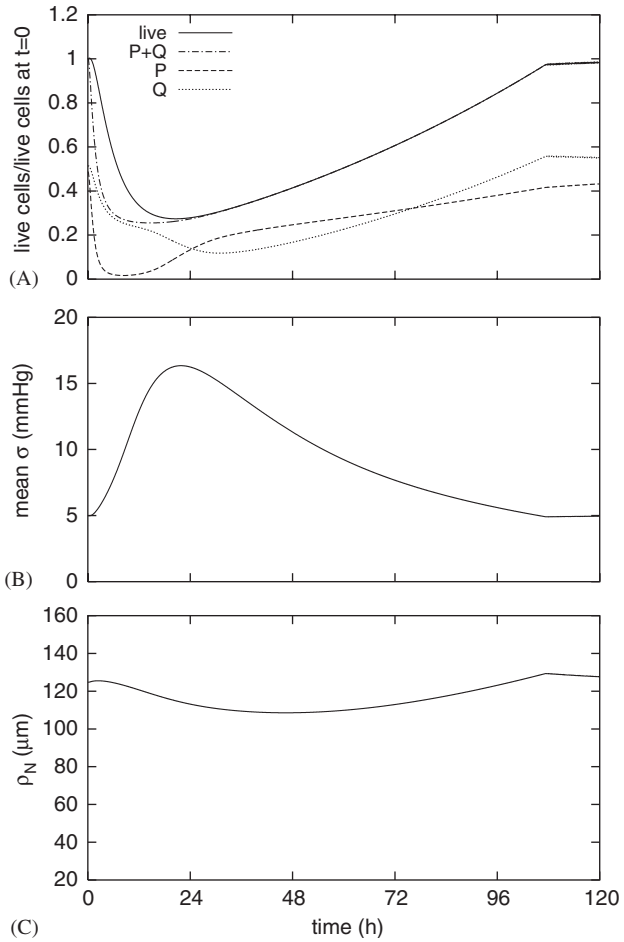

Fig. 4. Single-dose response: time course of live cells and undamaged subpopulations (A), of mean oxygen concentration (B) and of cord radius (C). The difference between live cells and $P + Q$ cells in panel A represents the time course of lethally damaged cells. Parameters as in Fig. 3 with $\lambda_{max}/\chi = 1$, $\mu = 0.25\,\mathrm{h}^{-1}$, $\mu_N = 0.02\,\mathrm{h}^{-1}$. Parameters of the treatment: $m_P = 4$ and $m_Q = 0.8$.

$v_Q(r,0))\,dr$ in the case of proliferating undamaged cells. We can see that the minimum of the undamaged cells $(P+Q)$ occurs at about 12 h, which is the time $(4\tau_1)$ when the damaging rates practically vanish. The decrease of live cells is instead delayed, according to the death rate constant μ. The decrement of the amount of live cells reduces oxygen consumption and thus causes a general reoxygenation of the cord as shown by the time course of the mean oxygen concentration (panel B). The increase of oxygen concentration results in higher values of the transition rate γ and lower values of λ, thus promoting recruitment of quiescent cells into proliferation. The effect of this recruitment is shown by the time course of the volume of proliferating and quiescent cells (see panel A). After an initial phase in which P cells are reduced far more than Q cells because of the cycle-specific effect of the drug, the recruitment from quiescence together with the ongoing proliferation produce a regrowth phase in which the proliferating population prevails over the quiescent population. This indicates the existence of a time window in which the cell population, as a whole, will become *more sensitive* to the activity of a cycle-specific drug than before the treatment (we remark that the P and Q subpopulations, in this simulation, have approximately the same sizes at $t=0$). Such phenomenon is not described in the model by Hahnfeldt et al. (2003), in which only the recovery of the pretreatment sensitivity is predicted. After this phase, the sensitivity reverts again, tending eventually to the steady-state value. Panel C reports the time evolution of the cord radius ρ_N, showing the initial cord regression followed by the regrowth. Immediately after the start of the evolution, the interface $r=\rho_N$ becomes material and so remains until it switches again to be nonmaterial during the regrowth phase with a slope discontinuity. The decrement of the cord radius contributes to the increase of oxygen concentration because of the boundary condition (15).

To elucidate how the sensitivity of the cell population to a cycle-specific drug changes in time for different scenarios of parameter values, we report the time course of the fraction of proliferating cells over the sum of proliferating and quiescent cells, that is,

$$\frac{P(t)}{P(t)+Q(t)}=\frac{\int_{r_0}^{\rho_N(t)} r v_P(r,t)\,dr}{\int_{r_0}^{\rho_N(t)} r(v_P(r,t)+v_Q(r,t))\,dr}. \tag{24}$$

Fig. 5 illustrates the effect of changes in the parameters of cell kinetics, that is, parameters of the functions $\lambda(\sigma)$ and $\gamma(\sigma)$, on the time course of the proliferating fraction given by (24). In all the panels, the continuous line represents the reference case (parameters as in Fig. 4). Panel A shows the effect of changing λ_{max} and γ_{max} ($\lambda_{min}=\gamma_{min}$ assumed equal to zero). When λ_{max} takes the lower value, the population is initially almost equally divided into proliferating and quiescent cells and, after an initial depletion of P cells, the oversensitization only occurs when γ_{max} has the greater value since the rate of recruitment is larger. On the contrary, when λ_{max} takes the higher value the initial fraction of P cells is lower (about 16%), and for both the chosen γ_{max} values the proliferating fraction appreciably increases, since even a limited number of recruited cells suffices to affect that fraction. Increasing γ_{max} makes this process more rapid. The position of the thresholds σ_Q and σ_P is found to be of major importance (panel B). When these thresholds are lowered to $\sigma_Q=5$ mmHg and $\sigma_P=10$ mmHg, cell resensitization is maximal because the reoxygenation is better exploited to recruit cells from quiescence. The opposite happens when the thresholds are increased. The effect of the width of the linear portion of the functions $\lambda(\sigma)$ and $\gamma(\sigma)$, changed while keeping constant the value of σ at which $\lambda=\gamma$, is shown in panel C. Although oversensitization occurs in all the cases examined, its extent is greater when the difference $\sigma_P-\sigma_Q$ is smaller.

Fig. 6 shows the effect of changes in the parameters related to the activity of the delivered drug. The curves of panel A were obtained by changing m_P, m_Q with m_Q/m_P constant, to simulate changes in drug dose. As expected, the resensitization is maximal (and very marked) with the high dose, the large cell death producing a quick and intense reoxygenation. The consequence of different sensitivities of the quiescent cells, i.e. of different m_Q values with m_P constant, are shown in panel B. The increase of the proliferating fraction after the treatment, as m_Q increases, is facilitated by the increase in the overall cell mortality. We remark, however, that for $m_Q=m_P$ the higher percentage of proliferating cells will not correspond to a higher sensitivity of the population to a second dose of the same (nonspecific) drug. A slower drug elimination at constant m_P, m_Q tends to dampen the increase of the proliferating fraction (panel C). This effect is also produced by a decrease of the death rate μ of the lethally damaged cells, as shown in panel D. When μ is small the minimum of living cells is achieved later and its value rises because of the concomitant cell repopulation, with the final effect of a delayed and reduced reoxygenation.

The existence of a time window, in which the proportion of proliferating cells in the population is greater than the pretreatment value, suggests that a second dose of a cycle-specific drug delivered in this time interval could be more effective than the first dose. In the next section we will investigate this possibility.

6. Split-dose response

We have compared the response of the cell population to a single bolus of drug (characterized by given m_P, m_Q), delivered at $t=0$, with the response to two half-dose boluses $(m_P/2, m_Q/2)$ delivered at $t=0$ and T. Fig. 7 illustrates a typical time course of the undamaged viable cells when $T=36$ h.

A criterion for comparing the effectiveness of different treatments is not univocally established. Thus the comparison was performed by using the following indices:

$$\text{Survival ratio}=\frac{\min[P_2(t)+Q_2(t)]}{\min[P_1(t)+Q_1(t)]}, \tag{25}$$

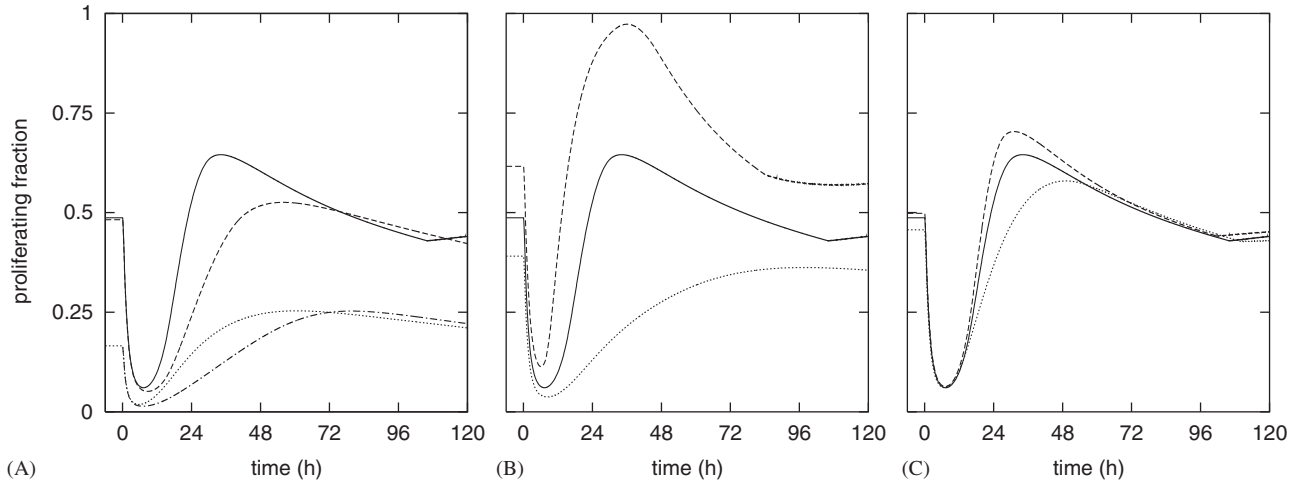

Fig. 5. (A) Effect of changes in λ_{max} and γ_{max} on the proliferating fraction: $\lambda_{max}/\chi = 1$ and $\gamma_{max}/\chi = 4$ solid line, $\lambda_{max}/\chi = 1$ and $\gamma_{max}/\chi = 1$ dashed, $\lambda_{max}/\chi = 4$ and $\gamma_{max}/\chi = 4$ dotted, $\lambda_{max}/\chi = 4$ and $\gamma_{max}/\chi = 1$ dashed-dotted. (B) Changes in σ_Q and σ_P: $\sigma_Q = 5$ and $\sigma_P = 10$ dashed, $\sigma_Q = 10$ and $\sigma_P = 15$ solid, $\sigma_Q = 15$ and $\sigma_P = 20$ dotted. (C) Changes in $\sigma_P - \sigma_Q$ with $\lambda = \gamma$ at $\sigma = 11$: $\sigma_P - \sigma_Q = 2.5$ dashed, $\sigma_P - \sigma_Q = 5$ solid, $\sigma_P - \sigma_Q = 30$ dotted. Other parameters as in Fig. 4.

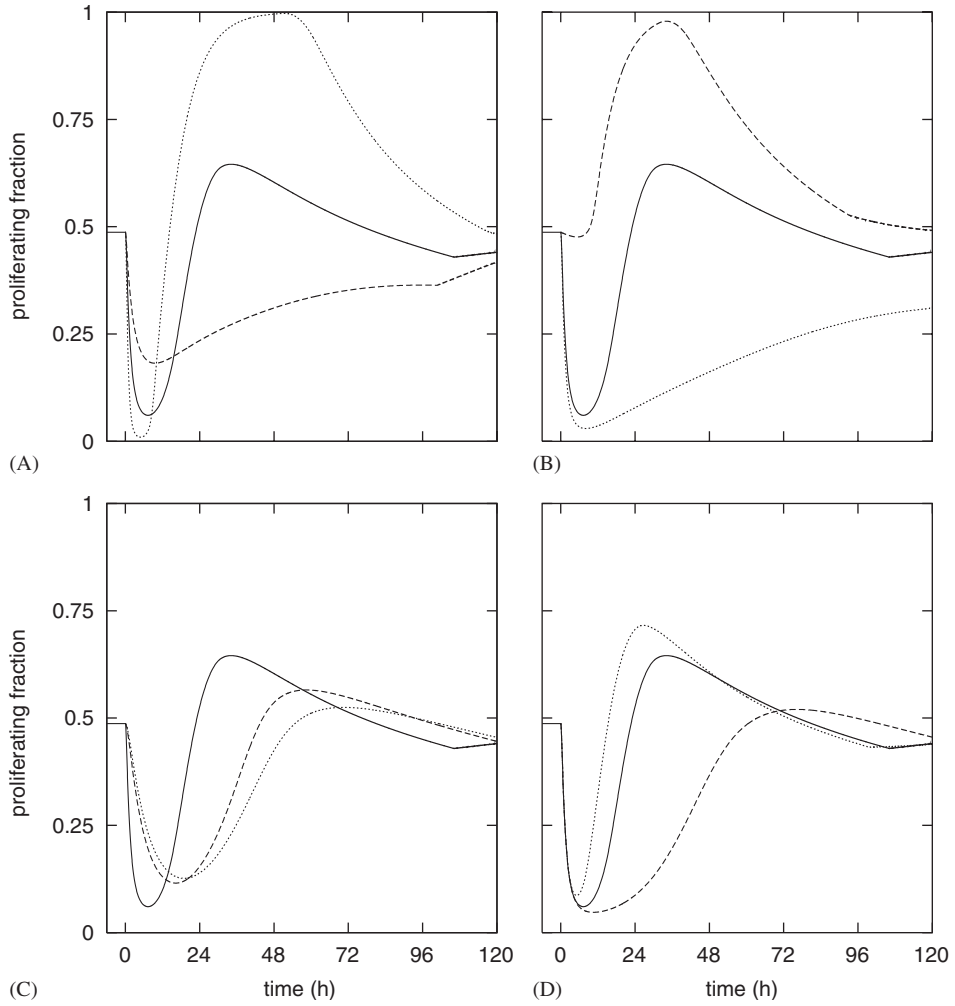

Fig. 6. (A) Effect of changes in m_P, with $m_Q = 0.2m_P$, on the proliferating fraction: $m_P = 2$ dashed, 4 solid, 8 dotted. (B) Changes in m_Q, with $m_P = 4$: $m_Q = 0$ dotted, 0.8 solid, 4 dashed. (C) Changes in τ_1 and τ_2: reference values, solid; reference values $\times 4$, dashed; reference values $\times 5$, dotted. (D) Changes in μ: $\mu = 1$ dotted, 0.25 solid, 0.0625 dashed. Other parameters as in Fig. 4.

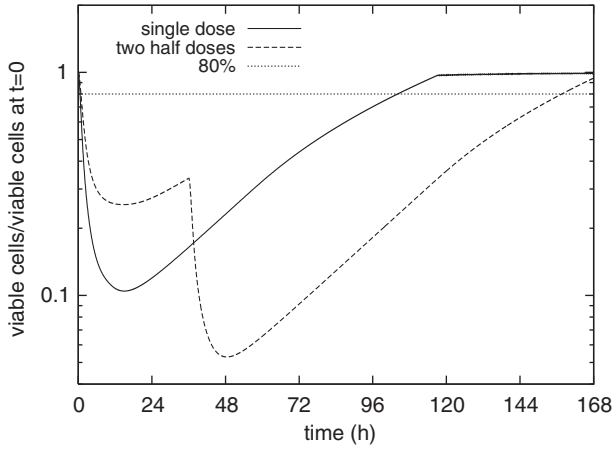

Fig. 7. Example of dose splitting. Undamaged viable cells after a single bolus at $t = 0$ (solid line) and after two half-dose boluses given at $t = 0$ and 36 h (dashed); $m_P = 8$, $m_Q = 1.6$, other parameters as in Fig. 4.

$$\text{Relative growth delay} = \frac{t80_2 - t80_1}{t80_1}, \tag{26}$$

where the subscripts 1, 2 refer to the single-dose response and to the split-dose response, respectively, and $t80$ is the time at which $P + Q$ regrows up to 80% of the initial value (see Fig. 7).

Fig. 8, panel A, shows the behaviour of the survival ratio as a function of the interfraction interval T. As expected, in coincidence with the time window in which cell oversensitization occurs this ratio is smaller than one. This shows the advantage of the dose splitting, with a more marked advantage at the higher dose. Instead, when the drug is not cycle-specific ($m_Q/m_P = 1$), the advantage obviously disappears even though the proliferating fraction of the cell population after the first dose is high in this condition (see Fig. 6B). We note that the survival ratio is less than one even with small interfraction intervals ($T = 6$–12 h), apparently in contrast with the strong depletion of the proliferating fraction at those times (see Fig. 5A). This fact can be explained by considering that the drug is active for a nonnegligible time interval (about 12 h in our simulations). Therefore, as noted by Hahnfeldt et al. (2003), also in the case of a single dose part of the dose actually affects a cell population that has become refractory. The results of Fig. 8A are paralleled by the behaviour of the relative growth delay (panel B). It can be surprising that when $T = 72$ h the growth delay induced by splitting the smaller dose does not decrease: in this case, although the cell population is no longer oversensitive, splitting the dose still produces a positive growth delay because of the saturating time course of $P + Q$.

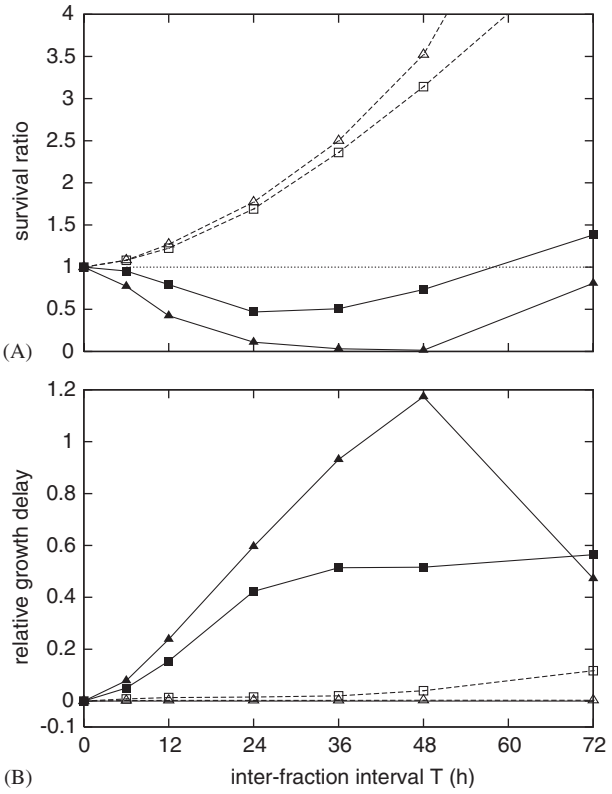

Fig. 8. Survival ratio (A) and relative growth delay (B) as a function of the time interval between the two fractions. Closed symbols: $m_Q/m_P = 0.2$; $m_P = 4$ for each fraction (squares), $m_P = 8$ (triangles). Open symbols: $m_Q/m_P = 1$; $m_P = 2$ (squares), 4 (triangles). Other parameters as in Fig. 4.

7. Effect of intervessel distance in the absence of necrosis

In many not too advanced tumours, the vessel density is high enough to guarantee an oxygenation level that prevents the formation of necrotic regions. We deal with this case by viewing the tumour as partitioned into adjacent, parallel and identical cylinders of tissue each surrounding a central vessel, as in the Krogh model of microcirculation. In addition, we assume that the vessels move solidly with the surrounding tissue, and are so displaced from the initial position during the evolution of the tumour mass (Bertuzzi et al., 2005a). We denote by $B(t)$ the radius of a generic tissue cylinder (cord). In the spirit of Krogh's approximation, the surface $r = B(t)$ prevents, due to the symmetry of the system, any exchange of matter with the neighbouring cords. In a regular hexagonal array of vessels, $2B$ represents the distance between the axes of two neighbouring vessels. Under these assumptions, the model described in Section 3 still holds with Eq. (15) replaced by

$$\left.\frac{\partial \sigma}{\partial r}\right|_{r=B(t)} = 0. \tag{27}$$

The cord boundary $B(t)$ will be a material boundary defined by

$$\dot{B} = u(B(t), t), \tag{28}$$

until $\sigma(B(t), t) > \sigma_N$.

In the absence of necrosis, supposing r_0 and σ_b unchanged, the mean oxygen level will be higher than in the cases in which necrosis is present and it is expected that, after the treatment, the reoxygenation will reach higher

levels with a consequent more marked increment of the proliferating fraction. We have simulated a possible initial state for the treatment by allowing the system to grow from the initial condition $v_P(r, t_0) = 1$, $r_0 \leqslant r \leqslant B(t_0)$, with $B(t_0)$ chosen such that $\sigma(B(t_0), t_0) > \sigma_P$. The initial state for the treatment was chosen when $\sigma(B(t), t)$ was equal to 5 mmHg; we obtained $B = 91.4\,\mu m$. Fig. 9A illustrates the time course of the proliferating fraction after a single dose of treatment. As compared with the corresponding case in which necrosis is present, the initial value of the proliferating fraction is higher (0.70 vs. 0.49) because of the higher level of oxygen concentration, and after the dose delivery the fraction reaches a value close to the unity. Panel B shows the time course of the mean oxygen concentration. This behaviour suggests that splitting the dose may be even more advantageous in this case than in the case in which necrosis is present. This prediction is confirmed by the results of Fig. 10 that show, for a given treatment dose, a reduced survival ratio and an increased growth delay in the case of absence of necrosis.

8. Concluding remarks

In the present paper we have studied the changes in the sensitivity of a tumour cell population to a cycle-specific drug, following the delivery of a single dose treatment. Our study utilizes a tumour cell population model with spatial structure, that incorporates oxygen diffusion and consumption and assumes that recruitment of quiescent cells into proliferation is stimulated by the increase of oxygen concentration. Because of the increase in oxygen concentration induced by the initial dose, the model predicts that a level of sensitivity greater than the pretreatment value may be attained in a time window after drug delivery. This fact implies that splitting the drug dose into two fractions separated by a suitable time interval may improve the efficacy of the treatment. Our simulations have only considered the case of two equal fractions, although to fully exploit the occurrence of oversensitization would require the study of an optimal fractionation strategy in which also the relative size of fractions is to be assessed. Fractionation of drug delivery is used in clinical chemotherapy with the aim of reducing the toxicity and then increasing the maximum tolerated dose (Moore and Erlichman, 1998). The present results highlight a possible additional advantage of fractionated schedules.

Although the oxygen concentration has been assumed to be the driving force of the transitions between proliferation and quiescence, the results of the present investigation should qualitatively hold even when cell kinetics is actually regulated by another chemical, provided that it is highly diffusible and consumed by live cells. Since, as it is well known, the cell sensitivity to radiations depends on the oxygen concentration, the dynamics of reoxygenation is

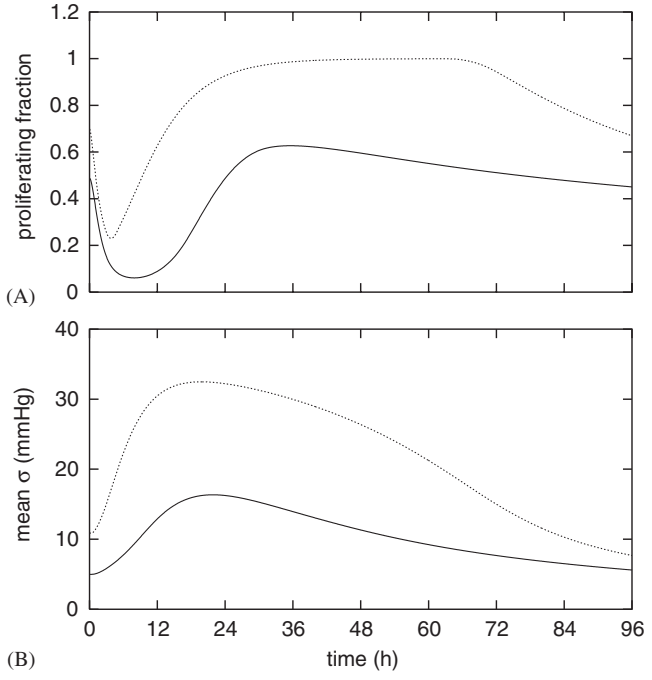

Fig. 9. Comparison of the response in the absence of necrosis (dotted lines) with the response in the presence of necrosis (reference case, solid lines). Time course, after a single dose of treatment, of the proliferating fraction (A) and of the mean oxygen concentration (B). Initial condition as specified in the text, parameter values as in Fig. 4.

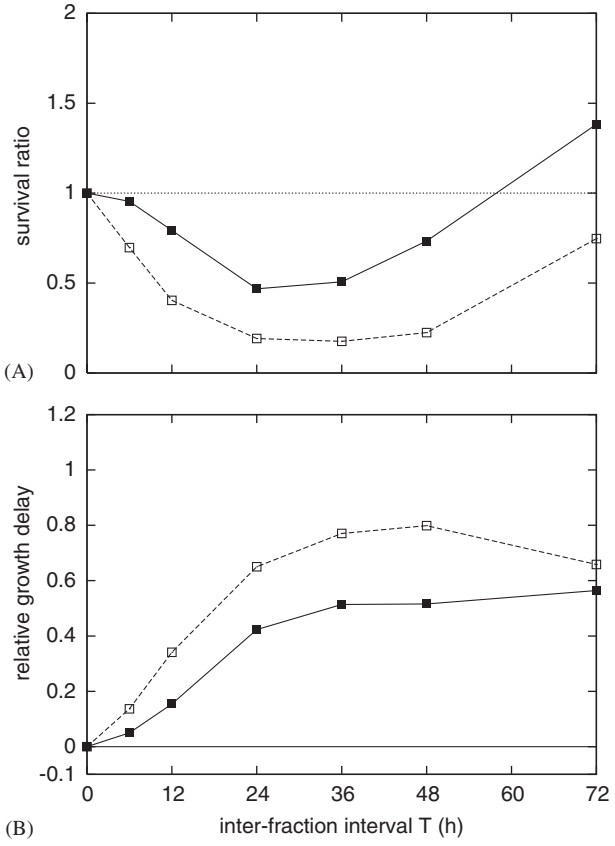

Fig. 10. Survival ratio (A) and relative growth delay (B) as a function of the time interval between the two fractions. Closed symbols, presence of necrosis; open symbols, absence of necrosis. $m_P = 4$ and $m_Q/m_P = 0.2$, other parameters as in Fig. 4.

important for assessing the time course of cell radiosensitivity. Thus our approach appears to be useful also in the context of radiotherapy, and this application will be presented in a forthcoming paper.

Some limitations of our model must be pointed out. The possible cell-cycle phase specificity of the drug has been disregarded since the cell cycle structure of the tumour cell population has not been accounted for. A more complete description of drug effects would in fact require a cell population model in which the proliferating subpopulation is structured in terms of cell age or cell maturity. Our analysis assumes that the treatment does not affect the tumour vasculature. Thus we are neglecting possible effects such as the increase of tumour perfusion related to the decompression of vessels in the presence of cell death (Griffon-Etienne et al., 1999; Araujo and McElwain, 2004). Finally, the model exploits an ideal geometry for the tumour tissue and its vasculature, that is, the tumour is viewed as an array of tumour cords whereas tumour vasculature is in general highly irregular and heterogeneous. It should be of interest to extend our approach to more realistic geometries. Some efforts to retain the discrete nature of vasculature in tumour modelling, with approaches different from that based on the Krogh cylinder model, have been presented with the aim of describing the distribution of oxygen (Secomb et al., 1993; Baish et al., 1996), the transport of drugs (McDougall et al., 2002), and the tumour evolution after treatment (Ribba et al., 2005).

Acknowledgement

This work was partially supported by the FIRB-MIUR Project "Metodi dell'Analisi Matematica in Biologia, Medicina e Ambiente".

Appendix A. A lower bound for v_P

From Eq. (18), the function $v_P(r)$ satisfies, for $r>\rho_P$, the following equation

$$\frac{\partial v_P}{\partial r}=\frac{1}{u(r)}\left[\chi v_P\left(1-\frac{v_P}{v^\star}\right)-\lambda(\sigma)v_P+\gamma(\sigma)(v^\star-v_P)\right], \quad (A.1)$$

with the boundary condition $v_P(\rho_P)=\hat{v}_P$. Since $\partial v_P/\partial r$ can be seen to be negative (see Bertuzzi et al., 2005b), we have

$$\frac{\partial v_P}{\partial r}\geqslant\frac{1}{\min_{r\in[\rho_P,\rho_N]}u(r)}\left[\chi v_P\left(1-\frac{v_P}{v^\star}\right)-\lambda_{max}v_P+\gamma_{min}(v^\star-v_P)\right]. \quad (A.2)$$

The quantity $ru(r)$ is nondecreasing in view of (19), thus $\min_{r\in[\rho_P,\rho_N]}u(r)\geqslant\rho_P u(\rho_P)/\rho_N$. Therefore we have $v_P(r)\geqslant v^\star\tilde{v}_P(r)$ with $\tilde{v}_P(r)$ given by

$$\frac{\partial\tilde{v}_P}{\partial r}=\alpha(-\tilde{v}_P^2+c_1\tilde{v}_P+c_2), \quad (A.3)$$

$$\tilde{v}_P(\rho_P)=\frac{\hat{v}_P}{v^\star}, \quad (A.4)$$

with

$$\alpha=\frac{2v^\star\rho_N}{\hat{v}_P(\rho_P^2-r_0^2)}, \quad (A.5)$$

$$c_1=1-\frac{\lambda_{max}+\gamma_{min}}{\chi}, \quad (A.6)$$

$$c_2=\frac{\gamma_{min}}{\chi}, \quad (A.7)$$

where $c_2\geqslant 0$. In the case $c_1=c_2=0$ the solution of (A.3)–(A.4) is given by

$$\tilde{v}_P(r)=\frac{1}{\frac{v^\star}{\hat{v}_P}+\alpha(r-\rho_P)}. \quad (A.8)$$

Excluding the above case, the r.h.s. of (A.3) can be rewritten as $\alpha(\eta_1-\tilde{v}_P)(\tilde{v}_P-\eta_2)$, where $\eta_{1,2}=\frac{1}{2}(c_1\pm\sqrt{c_1^2+4c_2})$, $\eta_1\geqslant 0$, $\eta_2\leqslant 0$, $\eta_1\neq\eta_2$. By comparing η_1 with $\hat{v}_P/v^\star$, as given by Eq. (20), and taking into account that $\hat{v}_P$ is a decreasing function of λ_{min} and is increasing with γ_{max}, and that $\lambda_{min}<\lambda_{max}$, we can see that $\eta_1<\hat{v}_P/v^\star$. Therefore $\tilde{v}_P(r)$ is decreasing. By integrating (A.3) with the boundary condition (A.4), we obtain

$$\tilde{v}_P(r)=\frac{\eta_1-\eta_2 A e^{-\alpha(\eta_1-\eta_2)(r-\rho_P)}}{1-Ae^{-\alpha(\eta_1-\eta_2)(r-\rho_P)}}, \quad (A.9)$$

where

$$A=\frac{\frac{\hat{v}_P}{v^\star}-\eta_1}{\frac{\hat{v}_P}{v^\star}-\eta_2}. \quad (A.10)$$

Functions (A.8) and (A.9), evaluated at $r=\rho_N$, yield the lower bound for $v_P/v^\star$. By rewriting (A.9)–(A.10) in terms of c_1 and c_2, and differentiating w.r.t. c_1 while keeping c_2 constant, it is easy to see that this bound is decreasing as λ_{max}/χ increases.

References

Alarcón, T., Byrne, H.M., Maini, P.K., 2004. A mathematical model of the effects of hypoxia on the cell-cycle of normal and cancer cells. J. Theor. Biol. 229, 395–411.

Åmellem, Ø., Pettersen, E.O., 1993. Cell-cycle progression in human-cells following re-oxygenation after extreme hypoxia—consequences concerning initiation of DNA-synthesis. Cell Prolif. 26, 25–35.

Araujo, R.P., McElwain, D.L.S., 2004. New insights into vascular collapse and growth dynamics in solid tumors. J. Theor. Biol. 228, 335–346.

Baish, J.W., Gazit, Y., Berk, D.A., Nozue, M., Baxter, L.T., Jain, R.K., 1996. Role of tumor vascular architecture in nutrient and drug delivery: an invasion percolation-based network model. Microvasc. Res. 51, 327–346.

Bakker, P.J.M., de Vries, R.J.L., Tukker, C.J., Hoede, R.A., Barendsen, G.V., 1993. Application of a DNA double labelling method for the flow cytometric analysis of recruitment of non-cycling cells in a mixed population of P and Q cells. Cell Prolif. 26, 89–100.

Bertuzzi, A., d'Onofrio, A., Fasano, A., Gandolfi, A., 2003. Regression and regrowth of tumour cords following single-dose anticancer treatment. Bull. Math. Biol. 65, 903–931.

Bertuzzi, A., Fasano, A., Gandolfi, A., 2004. A free boundary problem with unilateral constraints describing the evolution of a tumour cord under the influence of cell killing agents. SIAM J. Math. Anal. 36, 882–915.

Bertuzzi, A., Fasano, A., Filidoro, L., Gandolfi, A., Sinisgalli, C., 2005a. Dynamics of tumour cords following changes in oxygen availability: a model including a delayed exit from quiescence. Math. Comput. Model. 41, 1119–1135.

Bertuzzi, A., Fasano, A., Gandolfi, A., 2005b. A mathematical model for tumour cords incorporating the flow of interstitial fluid. Math. Mod. Meth. Appl. Sci. 15, 1735–1777.

Bredel-Geissler, A., Karbach, U., Walenta, S., Vollrath, L., Mueller-Klieser, W., 1992. Proliferation-associated oxygen consumption and morphology of tumor cells in monolayer and spheroid culture. J. Cell. Physiol. 153, 44–52.

Brenner, D.J., Hlatky, L.R., Hahnfeldt, P.J., Hall, E.J., Sachs, R.K., 1995. A convenient extension of the linear-quadratic model to include redistribution and reoxygenation. Int. J. Radiat. Oncol. Biol. Phys. 32, 379–390.

Byrne, H., Preziosi, L., 2003. Modelling solid tumour growth using the theory of mixtures. Math. Med. Biol. 20, 341–366.

Casciari, J.J., Sotirchos, S.V., Sutherland, R.M., 1992. Variations in tumor cell growth rates and metabolism with oxygen concentration, glucose concentration, and extracellular pH. J. Cell. Physiol. 151, 386–394.

Freyer, J.P., Sutherland, R.M., 1986a. Regulation of growth saturation and development of necrosis in EMT6/Ro multicellular spheroids by the glucose and oxygen supply. Cancer Res. 46, 3504–3512.

Freyer, J.P., Sutherland, R.M., 1986b. Proliferative and clonogenic heterogeneity of cells from EMT6/Ro multicellular spheroids induced by the glucose and oxygen supply. Cancer Res. 46, 3513–3520.

Friedman, A., 2004. A hierarchy of cancer models and their mathematical challenges. Discrete Contin. Dynam. Systems B 4, 147–159.

Griffon-Etienne, G., Boucher, Y., Brekken, C., Suit, H.D., Jain, R.K., 1999. Taxane-induced apoptosis decompresses blood vessels and lowers interstitial fluid pressure in solid tumors: clinical implications. Cancer Res. 59, 3776–3782.

Hahnfeldt, P., Hlatky, L., 1998. Cell resensitization during protracted dosing of heterogeneous cell populations. Radiat. Res. 150, 681–687.

Hahnfeldt, P., Folkman, J., Hlatky, L., 2003. Minimizing long-term tumor burden: the logic for metronomic chemotherapeutic dosing and its antiangiogenic bass. J. Theor. Biol. 220, 545–554.

Hirst, D.G., Denekamp, J., 1979. Tumour cell proliferation in relation to the vasculature. Cell Tissue Kinet. 12, 31–42.

Kozusko, F., Chen, P.H., Grant, S.G., Day, B.W., Panetta, J.C., 2001. A mathematical model of in vitro cancer cell growth and treatment with the antimitotic agent curacin A. Math. Biosci. 170, 1–16.

Lankelma, J., Fernandez-Luque, R., Dekker, H., Pinedo, H.M., 2003. Simulation model of doxorubicin activity in islets of human breast cancer cells. Biochim. Biophys. Acta 1622, 169–178.

Masunaga, S., Ono, K., Mitsumori, M., Abe, M., 1993. Alteration of radiosensitivity of quiescent cell populations in solid tumors irradiated with X-rays twice at various intervals. Jpn. J. Cancer Res. 84, 1130–1135.

Masunaga, S., Ono, K., Hori, H., Suzuki, M., Kinashi, Y., Takagaki, M., Kasai, S., Nagasawa, H., Uto, Y., 2000. Change in oxygenation status in intratumour total and quiescent cells following gamma-ray irradiation, tirapazamine administration, cisplatin injection and bleomycin treatment. Br. J. Radiol. 73, 978–986.

McDougall, S.R., Anderson, R.A., Chaplain, M.A.J., Sherratt, J.A., 2002. Mathematical modelling of flow through vascular networks: implications for tumour-induced angiogenesis and chemotherapy strategies. Bull. Math. Biol. 64, 673–702.

Montalenti, F., Sena, G., Cappella, P., Ubezio, P., 1998. Simulating cancer cell kinetics after drug treatment: application to Cisplatin on ovarian carcinoma. Phys. Rev. E 57, 5877–5887.

Moore, M.J., Erlichman, C., 1998. Pharmacology of anticancer drugs. In: Tannock, I.F., Hill, R.P. (Eds.), The Basic Science of Oncology. McGraw-Hill, New York, USA, pp. 370–391.

Moore, J.V., Hopkins, H.A., Looney, W.B., 1984. Tumour-cord parameters in two rat hepatomas that differ in their radiobiological oxygenation status. Radiat. Environ. Biophys. 23, 213–222.

Moore, J.V., Hasleton, P.S., Buckley, C.H., 1985. Tumour cords in 52 human bronchial and cervical squamous cell carcinomas: inferences for their cellular kinetics and radiobiology. Br. J. Cancer 51, 407–413.

Nakano, T., Oka, K., 1991. Transition of Ki-67 index of uterine cervical tumors during radiation therapy. Immunohistochemical study. Cancer 68, 517–523.

Neshasteh-Riz, A., Angerson, W.J., Reeves, J.R., Smith, G., Rampling, R., Mairs, R.J., 1997. Incorporation of iododeoxyuridine in multicellular glioma spheroids: implications for DNA-targeted radiotherapy using Auger electron emitters. Br. J. Cancer 75, 493–499.

Olive, P.L., 1994. Radiation-induced reoxygenation in the SCCVII murine tumour: evidence for a decrease in oxygen consumption and an increase in tumour perfusion. Radiother. Oncol. 32, 37–46.

Potmesil, M., Goldfeder, A., 1980. Cell kinetics of irradiated experimental tumors: cell transition from the non-proliferating to the proliferating pool. Cell Tissue Kinet. 13, 563–570.

Ribba, B., Marron, K., Agur, Z., Alarcòn, T., Maini, P.K., 2005. A mathematical model of Doxorubicin treatment efficacy on non-Hodgkin's lymphoma: investigation of current protocol through theoretical modelling results. Bull. Math. Biol. 67, 79–99.

Secomb, T.W., Hsu, R., Dewhirst, M.W., Klitzman, B., Gross, J.F., 1993. Analysis of oxygen transport to tumor tissue by microvascular networks. Int. J. Radiat. Oncol. Biol. Phys. 25, 481–489.

Sena, G., Onado, C., Cappella, P., Montalenti, F., Ubezio, P., 1999. Measuring the complexity of cell cycle arrest and killing of drugs: kinetics of phase-specific effects induced by taxol. Cytometry 37, 113–124.

Tannock, I.F., 1968. The relation between cell proliferation and the vascular system in a transplanted mouse mammary tumour. Br. J. Cancer 22, 258–273.

Zhao, M., Pipe, J.G., Bonnett, J., Evelhoch, J.L., 1996. Early detection of treatment response by diffusion-weighted ^{1}H-NMR spectroscopy in a murine tumour in vivo. Br. J. Cancer 73, 61–64.